In Situ FTIR ATR Spectroscopic Study of the Interaction of Immobilized Human Serum Albumin with Cholate in Aqueous Environment†

Norbert Hassler,‡ Dieter Baurecht,* Gerald Reiter,§ and Urs Peter Fringeli||

Institute of Biophysical Chemistry, University of Vienna, Althanstrasse 14, A-1090 Vienna, Austria

Received: June 25, 2010; Revised Manuscript Received: October 29, 2010

Fourier transform infrared (FTIR) attenuated total reflection (ATR) spectroscopy is increasingly used for the investigation of processes at or near interfaces. Exposing HSA dissolved in phosphate buffered saline (PBS) to a clean germanium (Ge) multiple internal reflection element (MIRE) led to the formation of a stable compact monolayer with a surface concentration of $(5.31 \pm 0.49) \times 10^{-12}$ mol cm^{-2}. Using a flow-through cuvette enabled in situ the monitoring of the HSA layer preparing and the interaction of this layer with a 5 mM solution of cholate in PBS. In order to achieve optimum sensitivity, two enhanced spectroscopic techniques have been applied: single-beam-sample-reference (SBSR) technique and concentration-modulated excitation (c-ME). Solutions of cholate and pure PBS were pumped alternatively with frequency ω through the sample compartment containing the immobilized HSA monolayer. Spectral changes due to interaction between cholate and HSA were now marked by the same frequency ω and could therefore be separated from the dominating unaffected part of the spectrum by phase-sensitive detection (PSD). It was found that at 5.0 mM bulk concentration of cholate 6.1 ± 1.0 cholate molecules were bonded by one immobilized HSA molecule. Furthermore, an increase of α-helical structures in HSA was initiated by cholate bonding.

Introduction

Human serum albumin (HSA) is a principal component of blood with a concentration of about 40 mg/mL. It is one of the most studied proteins and is mainly responsible for the maintenance of blood pH as well as for bonding and transporting many metabolites in the blood circuit.[1−3]

HSA is a monomeric protein with a molecular weight of 66.4 kDa. As found by X-ray studies, its three-dimensional shape can be approximated by an equilateral triangle with sides of ∼80 Å and a depth of ∼30 Å.[2] The main secondary structural element of albumin is the α-helix (67%), the amount of β-turns is 10%.[2] Although HSA has a high degree of conformational flexibility, its structure exhibits remarkable resistance against denaturation,[4] thus enabling long-term experiments in the laboratory. Albumins have a distinct tendency to adsorb as monomolecular film on hydrophilic surfaces.[5]

The most outstanding property of albumin is its ability to bond reversibly many different ligands, one of them is cholate, the anion of cholic acid occurring at the natural pH of blood.[1] Belonging to the bile acids, it is produced from cholesterol in the liver and stored in the gall bladder. Its main function is solubilization of lipids in the progress of digestion.

Cholate has a molecular weight of 430.6 g/mol and is a so-called natural detergent. Considering that its basic constitution is like cholesterol, the molecular structure reveals areas of hydrophobic and hydrophilic qualities, explaining the solubilizing properties by its stereochemical characteristics.[6] From equilibrium dialysis it is known that 1 mol HSA in solution can bond 2.8 mol of cholate with a bonding constant of 3300 and 12.0 mol with a bonding constant of 300.[7]

The interaction of albumin with substances like bilirubin, bile acids, and ammonia is also of medical interest. In case of liver failure these substances bonded to albumin have to be removed from the blood by an extracorporeal liver support system.[8]

In this study we have investigated the interaction of a 5 mM solution of cholate with an immobilized HSA monolayer adsorbed to a multiple internal reflection element (MIRE) by FTIR ATR spectroscopy to get quantitative information on effects initiated by specific bonding. The used experimental setup may also serve as a model reactor for artificial blood cleaning. In order to achieve a spectroscopic sensitivity above that of conventional difference spectroscopy, modulated excitation (ME) FTIR ATR spectroscopy was applied.[9] Excitation of HSA was performed by periodically exchanging cholate solution and pure buffer in the ATR cuvette. This type of ME is referred to as concentration-modulated excitation (c-ME) or concentration modulation.

Moreover, information on the long-term stability of the adsorbed HSA layer under hydrodynamic stress is also obtained. Since a thin coating of albumin on the surface of blood vessel grafts and vascular catheters reduces the adhesion and aggregation of platelets with subsequent thrombus formation,[10] the results are also of practical interest.

Experimental Methods

Materials. Human serum albumin (HSA; Sigma code: A3782) and sodium cholate (Na-Ch; C6445) were used as purchased from Sigma. Phosphate buffered saline (PBS) consisted of 10 mM Na_2HPO_4/NaH_2PO_4 pH 7.2, 150 mM NaCl, and 0.02% (*w*/*v*) sodium azide. All solutions were prepared with ultra pure water (Elga, U.S.A.) and degassed.

Instrumentation. FTIR spectra were recorded with a Bruker IFS 66 spectrometer at 4 cm^{-1} resolution and a zero filling factor

† Part of the "Alfons Baiker Festschrift".

* Corresponding author. Tel.: + 43-1-4277-52539. Fax: + 43-1-4277-9525. E-mail: dieter.baurecht@univie.ac.at.

‡ Current address: Ludwig Boltzmann-Institute for Osteology, Heinrich Collin-Strasse 30, 1140 Vienna, Austria.

§ Current address: Max Planck Institute of Colloids and Interfaces Research Campus Golm, Room 2.239, Am Mühlenberg 1, 14476 Potsdam-Golm, Germany.

|| Deceased on October 6th, 2008.

10.1021/jp105870z
Published on Web 12/13/2010

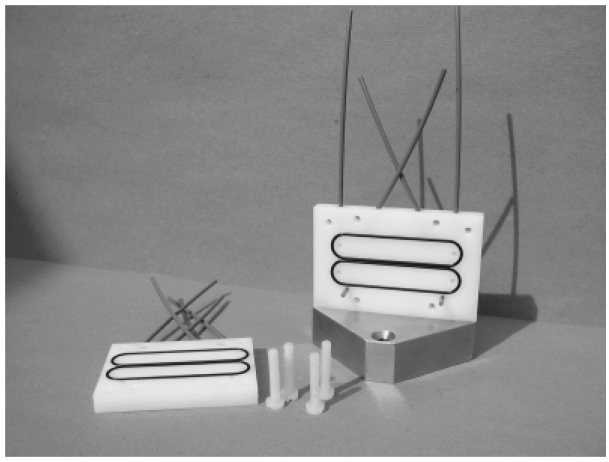

Figure 1. Flow-through cuvette used in this study. It was made of Delrin and consisted of four compartments, which were independently accessible by liquids and gases. Each compartment was sealed by a Viton O-ring and had a volume of about 80 μL. The Ge MIRE was mounted between the front and back part of the cuvette. Sample (S) and reference (R) compartments were placed above each other on either side of the MIRE. A computer controlled lift mounted on the ATR attachment enabled alternating measurements of single channel spectra in the upper and lower compartment of the MIRE by vertical displacement of the flow-through cuvette.

of 4. The measurement of double sided interferograms using Blackman-Harris 3-term apodization and power spectrum as Fourier transformation parameters was used to achieve best results at absorptions in the mAU range. The spectrometer purged with dry and carbon dioxide free air was equipped with an ATR attachment (OPTISPEC, Neerach, CH), a mercury−cadmium telluride (MCT) detector and an aluminum grid polarizer on a KRS-5 substrate (Specac, Orpington, U.K.), thus enabling measurements with parallel (pp) and perpendicular (vp) polarized IR light under computer control.

A trapezoidal germanium multiple internal reflection element (Ge MIRE) with dimensions of 52 × 20 × 2.0 mm^3 and an angle of incidence of $\theta = 45°$ was mounted in a hydrodynamically optimized flow-through cuvette made of Delrin (Figure 1).[11] Two sample (S) and two reference (R) compartments with a volume of about 80 μL each were placed above each other on either side of the MIRE. The geometry of the MIRE and the mean surface within two equivalent compartments corresponded to $N = 19.6$ active internal reflections. All compartments can be rinsed via Viton tubes connected to external peristaltic pumps (Ismatec, CH). All compartments were thermostatted at 25 °C by water circulation.

Single-Beam-Sample-Reference (SBSR) Method. A computer controlled lift mounted on the ATR attachment enabled quasi simultaneously measurements of single channel intensity spectra in the sample (I_S) and reference (I_R) compartments by a vertical displacement of the flow-through cuvette in a parallel IR beam. Since S and R are individually accessible by the single beam of the FTIR spectrometer, this technique is referred to as single-beam-sample-reference (SBSR) method. SBSR absorbance spectra were calculated from corresponding single channel spectra, i.e., $A = -\log(I_S/I_R)$. A total of 1000−2000 scans were accumulated to achieve the desired signal-to-noise ratio. For details and more applications of SBSR technique the reader is referred to refs 12−19.

Concentration-Modulated Excitation (c-ME). c-ME was performed by periodical altering of the concentration of cholate in the S compartments of the flow-through cuvette. Schematic setups of typical c-ME experiments are shown in refs 9 and 13. Before starting the modulation experiments, all compartments and all supplying tubes were filled with PBS and rinsed as long as there were no changes in in situ measured spectra. Afterward, the inlets of the sample compartments were filled with a 5.0 mM cholate solution. During the first half of a modulation period, a 5.0 mM solution of sodium cholate in PBS was pumped through the S compartments, while during the second half-period the S compartments were rinsed with pure PBS, using the same flow rate of 0.9 mL/min. Within one modulation period of $T = 9.8$ min, 32 single channel spectra, referred to as sample-point-spectra (SPS) were recorded by collecting 88 scans per SPS.

c-ME experiments were carried out with parallel (pp) and perpendicular (vp) polarized incident light in the sequence vp-pp-vp, i.e. one cycle consisted of two times of 6 averaged modulation periods measured with vp incident light and 6 averaged modulation periods measured with pp incident light in between. There were three reasons for this sequence. (i) The two vp spectra were used to analyze if there was any change during a single vp-pp-vp cycle. (ii) Co-addition and therefore doubling the number of vp spectra in case of proved stability led to the same S/N ratio of vp and pp spectra, due to 2/3 lower IR intensity of vp polarized light. (iii) The same mean age of coadded vp spectra compared to the pp spectra was achieved. Twenty-eight vp−pp−vp cycles have been measured in order to achieve the required S/N ratio. Moreover, at the beginning of each cycle, SBSR spectra have been measured also in a vp−pp−vp sequence in order to check the stationary surface concentration and structure of the layer.

To calculate time-resolved absorbance from single channel SPS, the geometric mean of all SPS was used as reference. Those absorbance spectra contain contributions of cholate bonded to the HSA layer, as well as dissolved in the bulk. In order to get the amount of cholate dissolved in the bulk, an additional modulation experiment was performed without a HSA layer. The difference between the resulting absorption bands gives the amount of cholate bonded to the HSA layer. The resulting time-resolved peak absorbancies of the $\nu_S(COO^-)$ vibrational band for cholate in bulk and the resulting amount of cholate bonded to the HSA layer are shown in Figure 2.

Additionally to conventional difference spectroscopy, the data were also processed by phase-sensitive-detection (PSD) according to eq 1. In an electronic sense this procedure enables narrow band signal detection, thus enhancing the S/N ratio.[9,20] In this application PSD was performed only in the fundamental frequency ($k = 1$). Moreover, for quantification of cholate bonded to HSA the following features of c-ME had to be considered: (i) Concentration modulation occurred between 0 and 5 mM, but the reference spectrum calculated as mean over all SPS corresponded to a mean cholate concentration of 2.5 mM. Since PSD gives access to the modulated amplitude of the absorption, the absorption amplitudes of the resulting phase-resolved spectra had to be multiplied by the factor 2 in order to represent the absorption difference caused by the 5 mM concentration change. (ii) During one modulation period ($T = 9.8$ min) the content of the compartments of the flow-through cuvette was exchanged about 25 times resulting in a nearly rectangular excitation function (Figure 2). Due to the used sinusoidal PSD, the amplitude of the phase-resolved absorbance spectrum of the fundamental frequency Fourier series is enhanced by a factor of $4/\pi$. Therefore, the measured phase resolved spectra had additionally to be divided by $4/\pi$. For details on data acquisition and manipulation the reader is referred to refs 21 and 22.

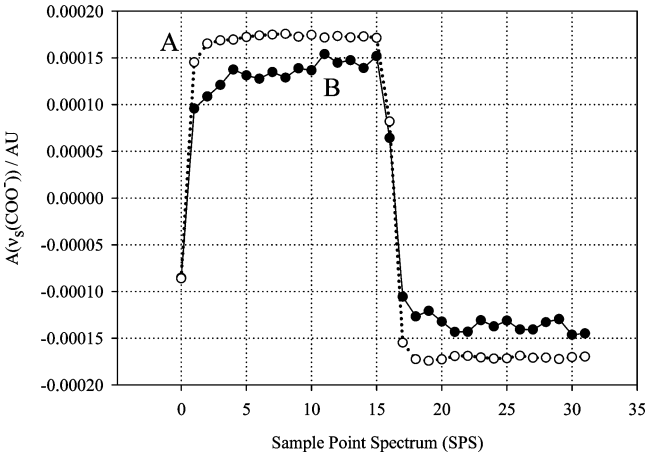

Figure 2. Time course of cholate absorbance averaged over all modulation periods evaluated from $\nu_s(COO^-)$ peak absorbance. (A) Cholate absorbance in the absence of the HSA layer (scaled down by a factor of 5). (B) Amount of cholate bonded to the HSA layer after subtraction of cholate absorption in the bulk. SPS were averaged over 28 modulation cycles with a period $T = 9.8$ min. The time course of the cholate concentration in the bulk was close to rectangular, while the cholate bonded to the HSA layer is slightly delayed in the response. Data result from spectra measured with pp incident light. As the mean of all SPS was used as reference spectrum, positive and negative absorbancies have to occur during the period.

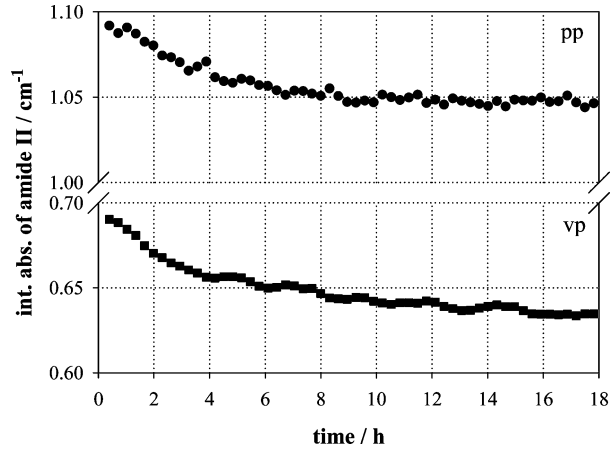

Figure 3. Time course of the stabilization of a human serum albumin (HSA) layer. Integrated absorbancies of the amide II vibration at 1547 cm^{-1} (integration range: 1600−1485 cm^{-1}) were evaluated from measurements with parallel (pp, ●) and perpendicular (vp, ■) polarized incident light. After spontaneous adsorption of HSA, the layer was rinsed with PBS pH 7.2 at a flow rate of 0.9 mL/min in order to remove loosely bonded molecules. A quasi-stable layer was achieved after about 16 h, resulting in a surface concentration of $\Gamma_{HSA} = (5.31 \pm 0.49) \times 10^{-12}$ mol cm^{-2}, which is slightly below a compact monolayer (see section Characterization of the Immobilized HSA Layer).

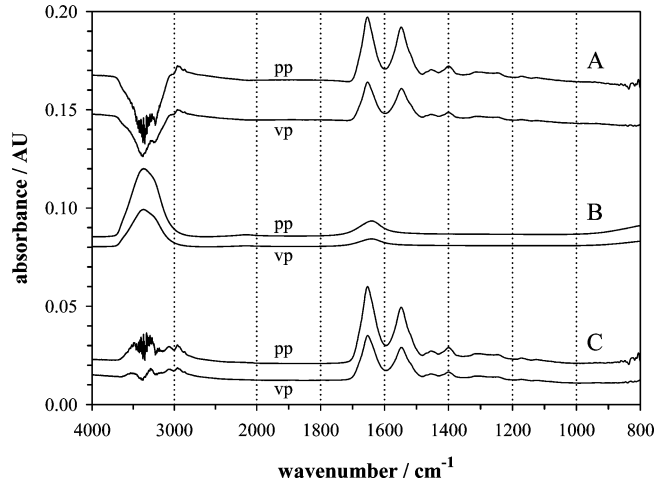

Figure 4. SBSR absorbance spectra of adsorbed HSA and of PBS pH 7.2 measured with parallel (pp) and perpendicular (vp) polarized incident light. (A) Absorbance of stable HSA layer in PBS before solvent compensation. Negative bands in regions of water absorption ($\nu(H_2O)$ 3350 cm^{-1}, $\delta(H_2O)$ 1640 cm^{-1}) resulted from PBS displacement by the layer in the S compartments, while in the R compartments PBS was in direct contact with the surface of the Ge MIRE, thus resulting in a more intense absorbance spectrum. (B) Absorbance of PBS pH 7.2 (reference: dry air) scaled by visual inspection to achieve optimum water compensation of spectra shown in (A). The corresponding layer thickness resulted in 17 Å. The layer of the displaced buffer might be somewhat thicker, since PBS may penetrate the layer and already exist as hydration water within it. Reference: air in empty R compartments. (C) Absorbance of HSA after solvent compensation. A perfect compensation of OH stretching and bending vibrations was not possible because of the presence of water bonded by protein molecules and free OH groups of amino acid residues as a part of HSA. Experimental conditions: Ge MIRE; $T = 25$ °C; angle of incidence $\theta = 45°$; number of active internal reflections $N = 19.6 \pm 1.0$. PBS: 10 mM Na_2HPO_4/NaH_2PO_4 pH 7.2, 150 mM NaCl, 0.02% (w/v) sodium azide; modulation period: $T = 9.8$ min; flow rate: 0.9 mL/min.

Adsorption of Human Serum Albumin (HSA). After filling sample and reference compartments with PBS, a solution of HSA (20.0 mg/mL in PBS) was pumped through the S compartments at a flow rate of 0.9 mL/min for 2.2 min exchanging the volume of the compartments 16 times. Finally, adsorption of HSA could complete in a flow-free state. A relatively high concentration of 20.0 mg/mL HSA was used, because the total quantity of dissolved HSA molecules in the S compartments was only 4.82×10^{-11} mol at this concentration, which corresponded to 1.5 times of molecules needed to achieve the final surface concentration of HSA. Since adsorption of HSA already started during the filling process, the amount of remaining molecules in the flow-free state was enough to achieve a stable layer. This was also verified by experiments with permanent HSA flow, where the dilution effect of the bulk concentration of 20.0 mg/mL turned out to be irrelevant with respect to the final surface concentration. After 5 h the adsorbed HSA layer was washed with PBS at a flow rate of 0.9 mL/min until stability of surface concentration was attained. Simultaneously, PBS was pumped through the R compartments at a flow rate of 50 μL/min. All steps were controlled by recording SBSR spectra with pp and vp incident light. The time course of the washing procedure is shown in Figure 3 and the final absorbance spectra of the HSA layer in Figure 4.

Quantification of Cholate. In all cases, quantification was based on the symmetric stretching vibration ($\nu_s(COO^-)$) at 1405 cm^{-1}. The integrated molar absorption coefficient of $\nu_s(COO^-)$ resulted in $\int \varepsilon(\tilde{\nu})\, d\tilde{\nu} = (1.36 \pm 0.14) \times 10^7$ cm mol^{-1} (range of integration: 1484 ± 3 to 1350 ± 3 cm^{-1}) as determined from a dilution series of bulk concentrations in the range of 1 mM to 6 mM cholate in PBS.

Determination of Critical Micellar Concentration (cmc) of Cholate. The cmc of cholate dissolved in PBS buffer was determined by tensiometry (Kruess Digital Tensiometer K10ST) using the Wilhelmy plate method at a temperature of 25 °C.

Theoretical Part. ***Modulated Excitation (ME) Spectroscopy.*** Modulated excitation spectroscopy, also referred to as modulation spectroscopy, is a sensitive technique to investigate reversible processes. The method is based on the excitation of the system by a periodic alteration of an external parameter, such as temperature,[23] pressure, electric field,[24] or concentration.[25,26] A system that shows reversible concentration changes regarding

the used excitation parameter will respond with periodically concentration changes with the frequency of the excitation and possibly also with higher harmonics. The latter occurs if the waveform of the excitation function also includes components with higher harmonics or if there is a nonlinear response of the system itself.

At the beginning of a ME experiment the system will relax from its equilibrium state to a new steady-state defined by the mean value of the excitation parameter. During this relaxation modulated excitation has to be performed without collection of data (dummy periods). After reaching the new quasi stationary state, data acquisition may begin by measuring N spectra at equidistant time slices within each repetitive excitation period T (sample point spectra, SPS). Thus time-dependent absorbance spectra of the continuous sample response $A(\tilde{\nu},t)$ are digitized (Figure 2). $A(\tilde{\nu},t)$ is then subjected to a discrete phase-sensitive detection (PSD) resulting in the so-called phase-resolved or demodulated spectra according to eq 1

$$A_k^{\phi_k^{\mathrm{PSD}}}(\tilde{\nu}) = \frac{2}{T}\int_0^T A(\tilde{\nu},t)\,\sin(k\omega t + \phi_k^{\mathrm{PSD}})\,\mathrm{d}t \qquad (1)$$

In a general case, $A(\tilde{\nu},t)$ may be a superposition of partial responses in the fundamental ω as well as in higher harmonics $k\omega$ according to eq 2

$$A(\tilde{\nu},t) = \sum_k A_{k_0}(\tilde{\nu})\,\sin(k\omega t + \phi_k) \qquad (2)$$

Introducing eq 2 into eq 1 results after integration[21] in

$$A_k^{\phi_k^{\mathrm{PSD}}}(\tilde{\nu}) = A_{k_0}(\tilde{\nu})\,\cos\,(\phi_k - \phi_k^{\mathrm{PSD}}) \qquad (3)$$

Equations 1−3 explain the principal features of PSD. The periodic stationary sample response $A(\tilde{\nu},t)$ has to be multiplied by a demodulation function. In case of eq 1 demodulation occurs at frequency $k\omega$. Moreover, a new arbitrary parameter ϕ_k^{PSD} is introduced. As a consequence, this procedure extracts the amplitude of the sample response with frequency $k\omega$ from the overall signal resulting in phase-resolved spectra described by eq 3. ϕ_k denotes the phase delay of the $k\cdot\omega$ sample response with respect to the onset of simulation. In case of a harmonic excitation, a sample response at frequencies with $k \neq 1$ unambiguously points to nonlinear steps in the reaction scheme of the system. ME spectroscopy may also give access to the reactive scheme when the period of the excitation frequency is in the same order of magnitude as the time constants of the reaction process. In this case, phase delays ϕ_k and the amplitudes of the responses A_k of single absorption bands (components k) are different. If the period of excitation is long compared to relaxation times of the system, there remains still a relevant advantage of ME spectroscopy over conventional difference spectroscopy: The signal-to-noise ratio and background compensation of a phase-resolved spectrum is much better compared to conventional difference spectroscopy. Almost all frequency components of the noise and of the background absorption (except the frequency components of the excitation frequency) are suppressed by the PSD. The reader is referred to refs 9, 21, and 22 for a more detailed description of ME spectroscopy.

Background Compensation with Respect to the Bulk Solution. In our measurement cholate can contribute to the overall absorbance spectra as dissolved substance in the bulk, as well as bonded to HSA. Separation of the corresponding components requires the knowledge of the absorbance of dissolved cholate without HSA layer. Unlike to transmission (T) spectroscopy, an accurate separation cannot be performed by simple subtraction of corresponding ATR spectra, due to the wavelength dependent penetration depth in ATR spectroscopy. Thus, the shape of an absorbance spectrum of a thin layer of dissolved cholate is different from the shape of a bulk absorbance spectrum of dissolved cholate. As a consequence, a scaled subtraction has to be applied. The evanescent field of the IR beam penetrates proportionally to its wavelength into the rarer medium as expressed by eq 4

$$d_{\mathrm{p}}(\tilde{\nu}) = \frac{1}{2\pi\tilde{\nu}\sqrt{{n_1}^2\sin^2\theta - {n_3}^2}} \qquad (4)$$

$d_{\mathrm{p}}(\tilde{\nu})$ denotes the so-called penetration depth at the wavenumber $\tilde{\nu} = 1/\lambda$. Further parameters are the wavelength, λ, the angle of incidence, θ, and the refractive indices, n_1 and n_3, of the MIRE and the bulk solution, respectively.

As long as the system behaves as weak absorber, i.e., the Napierian absorption index κ of the complex refractive index $\hat{n} = n + i\kappa$ fulfills the condition $\kappa < 0.1$, quantitative analysis may be based on the concept of effective thickness as introduced by Harrick.[27] The procedure has been further developed and applied to thin layers in refs 12 and 28. The effective thickness d_{e} represents a hypothetical thickness for a transmission cuvette which would result the same absorbance as experimentally obtained from one internal reflection in the ATR mode. For a bulk (b) isotropic (iso) rarer material in contact with the MIRE one obtains

$$d_{\mathrm{e,b}}^{\mathrm{iso}} = \frac{n_3}{n_1\cos\theta}\frac{d_{\mathrm{p}}}{2}{E_{\mathrm{r,b}}}^2 \qquad (5)$$

Equation 5 holds for parallel and perpendicular polarized incident light depending on the relative electric field strength $E_{\mathrm{r,b}}$ in the bulk (b) rarer medium, which results from Fresnel's equations. It should be noted that such a simple expression for the effective thickness holds only for polarized light. An approximation for unpolarized incident light has been derived in ref 12.

Since E_{r} declines exponentially with the distance z from the interface

$$E_{\mathrm{r}} = E_{\mathrm{r},0}\,\mathrm{e}^{-z/d_{\mathrm{p}}} \qquad (6)$$

eq 5 converts by linearization to eq 7 in case of a very thin ($d \ll d_{\mathrm{p}}$) isotropic surface layer (th) of thickness d, where n_2 is the refractive index of the layer

$$d_{\mathrm{e,th}}^{\mathrm{iso}} = \frac{n_2}{n_1\cos\theta}d{E_{\mathrm{r,th}}}^2 \qquad (7)$$

For adequate background compensation it follows from eqs 5 and 7 that the absorbance spectrum of the solvent has to be scaled by the wavenumber dependent factor κ and then added to the absorbance spectrum of the thin layer, thus removing the wavenumber dependent overcompensation of the background.

$$\kappa = \frac{d_{e,th}^{iso}}{d_{e,b}^{iso}} = \frac{2d}{d_p} = 4\pi\tilde{\nu}d\sqrt{n_1^2 \sin^2\theta - n_3^2} \quad (8)$$

For details, the reader is referred to ref 19.

Orientation Measurements. A prerequisite for orientation measurements is the existence of at least two measurements performed with different light polarizations. Generally, parallel (pp) and perpendicular (vp) polarized incident light is used. The basic quantity for data analysis is the so-called dichroic ratio R

$$R(\tilde{\nu}) = \frac{\int A_{pp}(\tilde{\nu})\, d\tilde{\nu}}{\int A_{vp}(\tilde{\nu})\, d\tilde{\nu}} \quad (9)$$

$\int A_{pp}(\tilde{\nu})\, d\tilde{\nu}$ and $\int A_{vp}(\tilde{\nu})\, d\tilde{\nu}$ denote the integrated absorbancies of a given absorbance band measured with pp and vp polarized incident light, respectively. Peak absorbancies may also be used instead of integrated absorbancies. Assuming a liquid crystalline ultrastructure (LCU) of the sample with uniaxial orientation along the normal to the MIRE (z axis), one obtains for the dichroic ratio the following expression:[28]

$$R(\tilde{\nu}) = \frac{\int A_{pp}(\tilde{\nu})\, d\tilde{\nu}}{\int A_{vp}(\tilde{\nu})\, d\tilde{\nu}} = \frac{E_x^2}{E_y^2} + 2\frac{E_z^2\overline{\langle\cos^2\Theta\rangle}}{E_y^2(1 - \overline{\langle\cos^2\Theta\rangle})} \quad (10)$$

where $\overline{\langle\cos^2\Theta\rangle}$ denotes the average over the mean squares of the cosines of the angles between transition moments of a given vibration and the z axis of the laboratory coordinate system, which is fixed to the MIRE. The xy plane is parallel to the surface of the MIRE, with the x axis directing along the light propagation. For details the reader is referred to ref 28.

Determination of Surface Concentration. The volume concentration c and the surface concentration Γ are related to each other via the thickness d of the sample. By introducing Lambert−Beer's law one obtains

$$c = \frac{\Gamma}{d} = \frac{\int A(\tilde{\nu})\, d\tilde{\nu}}{Nnd_e^{th}\int \varepsilon(\tilde{\nu})\, d\tilde{\nu}} \quad (11)$$

$\int A(\tilde{\nu})\, d\tilde{\nu}$ denotes the integrated absorbance of a distinct absorbance band measured with parallel (pp) or perpendicular (vp) polarized incident light, respectively. N and n are the mean numbers of the active internal reflections and equal functional groups per molecule. d_e^{th} is the effective thickness of the layer which depends on the polarization.[28] $\int \varepsilon(\tilde{\nu})\, d\tilde{\nu}$ denotes the common integrated molar absorption coefficient of the band. The surface concentration Γ may then be expressed as a function of the experimentally determined dichroic ratio R and the relative electric field strengths resulting from Fresnel's equations

$$\Gamma = \frac{d\int A(\tilde{\nu})\, d\tilde{\nu}}{3Nnd_{e,th}^{iso}\int \varepsilon(\tilde{\nu})d\tilde{\nu}}\left[2 - \frac{E_x^{r2}}{E_z^{r2}} + R_{exp}\frac{E_y^{r2}}{E_z^{r2}}\right] \quad (12)$$

The surface concentration Γ as given by eq 12 may be understood as the projection of the molecules in the volume defined by unit area and height d (real sample thickness). $d_{e,th}^{iso}$ denotes the effective thickness for an isotropic layer of real thickness d, as introduced by eq 7. In case of a thin layer $d_{e,th}^{iso}$ in eq 12 can be replaced by the relative effective thickness $d_e^{rel,iso} = d_{e,th}^{iso}/d$ depending on optical parameters only.[29]

$$\Gamma = \frac{\int A(\tilde{\nu})\, d\tilde{\nu}}{3Nnd_e^{rel,iso}\int \varepsilon(\tilde{\nu})\, d\tilde{\nu}}\left[2 - \frac{E_x^{r2}}{E_z^{r2}} + R_{exp}\frac{E_y^{r2}}{E_z^{r2}}\right] \quad (13)$$

As a consequence, surface concentration of a thin layer ($d \ll d_p$) featuring uniaxial orientation along the z-axis can be determined without knowing the real thickness d and its real structure.

Input parameters used for calculations, such as the angle of incidence, refractive indices, integrated molar absorption coefficients, and the number of active internal reflections are listed in Table 1.

Results and Discussion

Characterization of the Immobilized Human Serum Albumin (HSA) Layer. Adsorption of proteins belongs to an intensively investigated field because of its great importance in medicine, industry, and all natural sciences.[30−34] Results of adsorption experiments depend on temperature, pH, and composition of the solvent, as well as on the amino-acid sequence of the protein and the surface where adsorption takes place.[35−38] Theoretical background about adsorption is provided in ref 39. Kurrat et al.[40] assume that the formation of hydrogen bonds is responsible for HSA adsorption to Si and Ti surfaces.

As Ge exhibits a similar surface under our experimental conditions we assume the same mechanism for the HSA adsorption in our system. After adsorption of HSA to the Ge reflection element, the protein layer was rinsed with PBS for about 18 h to remove loosely attached HSA molecules (Figure 3). Absorbance spectra of a stable HSA layer in PBS are shown in Figure 4A. The maxima of the amide I and II bands are found at 1653 and 1548 cm^{-1}, respectively, pointing to a predominantly helical structure.[41] This finding is in accordance with X-ray studies.[2] Figure 4A reveals negative bands in regions of water absorption ($\nu(H_2O)$ 3350 cm^{-1}, $\delta(H_2O)$ 1640 cm^{-1}). This effect is referred to as overcompensation resulting from the fact that in the reference compartments PBS was in direct contact with the Ge MIRE, while in the presence of HSA, PBS was partly displaced by the layer. For solvent compensation the procedure described in the theoretical part "background compensation" was applied. Figure 4B represents absorbance spectra of PBS scaled to an estimated HSA layer thickness of 17 Å, which was found to result optimum background compensation. These spectra are dominated by the water absorption bands, because air was used as a reference. Addition of the spectra (Figure 4A and Figure 4B) resulted in the solvent compensated protein layer spectra, shown in Figure 4C. The thickness of 17 Å reflects the lowest limit of the HSA layer thickness, because most probably the HSA layer still enables some penetration of PBS. Moreover, water bonded by protein molecules as well as free OH groups of amino acid residues contributed to these spectral regions, too. As a consequence, a perfect compensation of OH stretching and bending vibrations is not possible.

The surface concentration of HSA at the end of the washing procedure, as calculated from integrated absorbancies of the amide II band (Figure 4C), resulted in $\Gamma_{HSA} = (5.40 \pm 0.50) \times 10^{-12}$ mol cm^{-2}. A small loss of HSA resulting from subsequent

TABLE 1: Magnitudes and Uncertainties of Input Parameters

parameter	symbol	magnitude	uncertainty[a]
angle of incidence/deg	θ	45.00	1.50
refractive index of germanium MIRE	n_1	4.00	<0.005
refractive index of an adsorbed protein layer	n_2	1.45	0.05
refractive index of the aqueous environment at 1547 cm^{-1}/at 1405 cm^{-1}	n_3	1.33/1.31	0.05
integrated molar absorption coefficient of amide II/(cm/mol);[46] linear baseline; range of integration: 1585 ± 1 − 1500 ± 1 cm^{-1}	$\int \varepsilon_{\text{amide II}}\, d\tilde{\nu}$	8.25×10^6	2.90×10^5
integrated molar absorption coefficient of $\nu_s(COO^-)$ of cholate in PBS/(cm/mol); linear baseline; Range of integration: 1484 ± 3 − 1350 ± 3 cm^{-1}	$\int \varepsilon_{(COO^-)}\, d\tilde{\nu}$	1.36×10^7	1.36×10^6
number of active internal reflections	N	19.6	1.0
number of equal functional groups per cholate molecule	n	1	0

[a] The limit of confidence corresponds approximately to 90%.

cholate modulation lead to an interpolated HSA concentration of $\Gamma_{0,HSA} = (5.31 \pm 0.49) \times 10^{-12}$ mol cm^{-2} or 0.352 $\mu g/cm^2$ at the begin of the modulation experiment (see below). Kurrat et al.[40] achieved HSA surface concentrations of 0.17 and 0.07 $\mu g/cm^2$ on hydrated titania in HEPES pH 7.4 buffer and PBS pH 7.4, respectively. They used HSA solutions with a concentration of about 80 μg/mL for adsorption. Differences to our results may be explained by the fact that surface concentrations are also dependent on the concentration of the protein solution.[42] Contrary to the experiments of Kurrat et al.[40] where adsorbed HSA was removed by subsequent washing with pure PBS, the surface concentration in our experiments was only decreased by 5% under same conditions.

The determined experimental value may also be compared with theoretical surface concentrations based on X-ray data. The three-dimensional shape of HSA may be approximated by an equilateral triangle with sides of ~80 Å and a depth of ~30 Å.[2] Two extreme cases of adsorption are considered: (i) HSA molecules adsorb with the lateral surface which would result in 80 × 30 Å = 2400 A^2 per molecule corresponding to a surface concentration of $\Gamma_{max} \approx 6.9 \times 10^{-12}$ mol cm^{-2}. (ii) Molecules adsorb with the triangle base plane and occupy an area of about 2770 $Å^2$ per molecule, which would correspond to a surface concentration of $\Gamma_{min} \approx 6.0 \times 10^{-12}$ mol cm^{-2}. As a consequence, the experimentally determined surface concentration indicates that the coverage on the MIRE is close to a monolayer. Accessibility of HSA during a modulation experiment should therefore not be hindered by multilayer formation, however, lateral hindrance could still play a role.

Concerning the mean orientation of α-helical segments, the analysis was based on the dichroic ratio of the amide II band according to section "orientation measurements", and resulted in $R_{exp}(HSA) = 1.63 \pm 0.12$. The uncertainty of this value is within the expected dichroic ratio for an isotropic thin layer, i.e., $R_{iso,th} = 1.67 \pm 0.12$ (Ge MIRE, $\theta = 45°$, $n_1 = 4.0$, $n_2 = 1.45$, $n_3 = 1.33$). As a consequence, α-helical segments in the HSA layer are expected to be arranged isotropic, or in a manner that results in a mean orientation with respect to the z-axis corresponding to the magic angle of $\theta_{mag} = 54.7°$. The latter, however, is unlikely.

Absorbance Spectra of Cholate. Absorbance spectra of a 5 mM cholate solution in PBS are shown in Figure 5A. The most prominent bands are the asymmetric (ν_{as}) and symmetric (ν_s) stretching vibrations of the COO^- group at 1544 and 1405 cm^{-1}, respectively. The slightly negative water bending band at 1635 cm^{-1} results from PBS (water) dilution by dissolved cholate, because pure PBS was used as reference. Since $\nu_{as}(COO^-)$ interferes with the water bending band, $\nu_s(COO^-)$ was used for quantitative analysis.

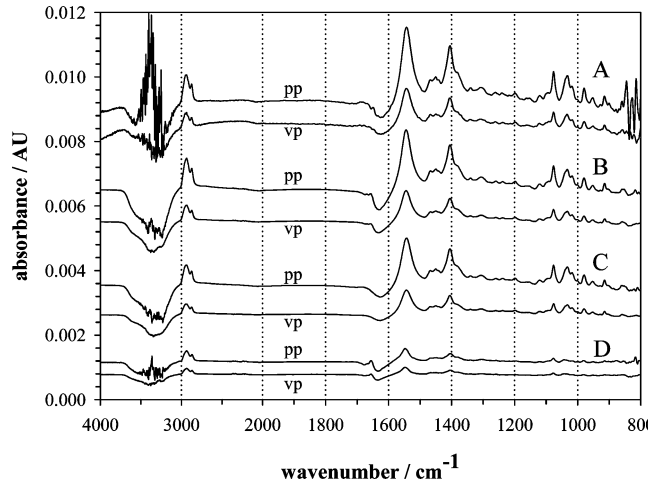

Figure 5. SBSR absorbance spectra measured with parallel (pp) and perpendicular (vp) polarized incident light. (A) SBSR spectra of 5.0 mM cholate dissolved in PBS pH 7.2. Pure PBS served as reference in the R compartments. The most prominent bands are $\nu_{as}(COO^-)$ at 1544 and $\nu_s(COO^-)$ at 1405 cm^{-1}. The latter was used for quantification of cholate. (B) and (C) phase-resolved spectra resulting from concentration-modulated excitation (c-ME) by 5 mM cholate in presence of the HSA layer (B) and in absence of the layer (C). According to eq 3 ϕ^{PSD} was set in such a way that $(\phi - \phi^{PSD}) = 0$, in order to maximize absorbance amplitude in phase-resolved spectra. Amplitudes of spectra are scaled to time zero, i.e., the beginning of the modulation experiments, to eliminate disturbances by HSA aging and detachment from the layer. (D) Difference between spectra B and C, reflecting reversible cholate bonding to HSA and structural responses of HSA upon interaction with cholate. An expanded scale presentation of the amide I and II region is given in Figure 6. Experimental conditions as described in Figure 4.

Cholate is known to form micelles of small size (2−3 molecules) above a critical micellar concentration (cmc) of 11 mM in 150 mM NaCl.[43] Under our experimental conditions cmc of the PBS resulted in (6.8 ± 0.2) mM (25 °C) indicating that a monomeric cholate solution has to be expected at the actual concentration of 5.0 mM.

Concentration-Modulated Excitation (c-ME) Experiments. c-ME of an adsorbed HSA layer by 5 mM cholate, as well as the reference experiment without HSA layer, were performed according to section "concentration-modulated excitation" of experimental methods. Since no time-resolved separation (phase-shifts) of absorption bands can be expected due to the low modulation frequency of 1.7 mHz, ϕ^{PSD} of the presented modulation spectra was adjusted in such a way that according to eq 3 $\phi - \phi^{PSD} = 0$, thus resulting in maximum amplitude of bands of all absorbing components. Figure 5B represents the superimposed phase-resolved absorbance of cholate interacting with the HSA layer and of cholate in the bulk phase. In order

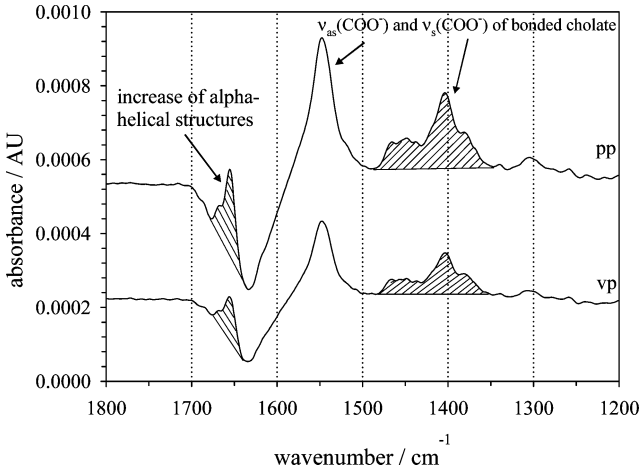

Figure 6. Phase-resolved absorbance changes of the HSA layer due to c-ME by 5 mM cholate in the region of amide I and II and COO^- absorbance (detail of Figure 5). Modulating the bulk surface concentration of cholate between 0 and 5 mM resulted in the shown phase resolved spectrum exhibiting positive absorbances of $\nu_{as}(COO^-)$ and $\nu_s(COO^-)$ of bonded cholate and negative absorbance of $\delta(H_2O)$. In addition a narrow positive band at 1656 cm^{-1}, most likely resulting from increasing of α-helical structures of HSA, appears. This band appears synchronously with the bands corresponding to cholate bonding to HSA because both bands show the same sign. A tentative interpretation is that α-helical structures of HSA were increased upon cholate bonding. Range of integration of the amide II band: 1600−1485 cm^{-1}. Range of integration of $\nu_s(COO^-)$: 1484−1350 cm^{-1}. Other experimental conditions as described in Figure 4.

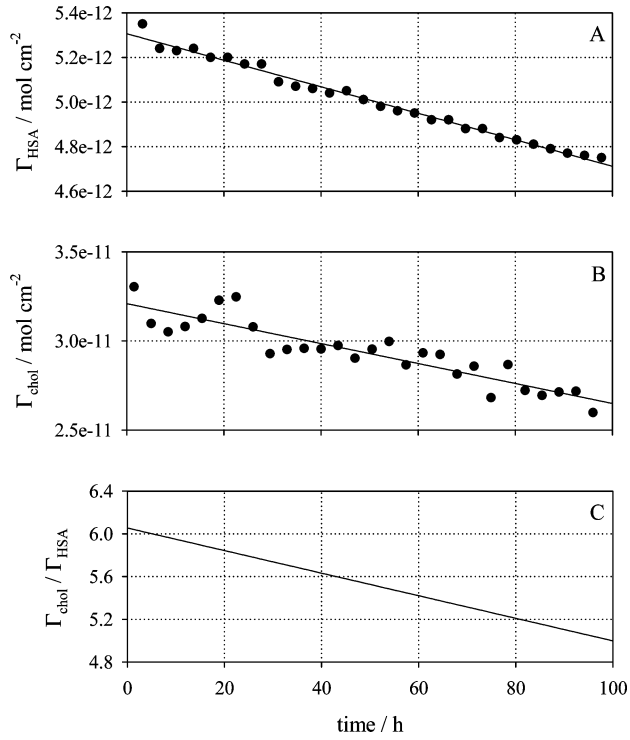

Figure 7. Time dependent decrease of surface concentrations of immobilized HSA (A), of cholate reversibly bonded to adsorbed HSA (B), and of the bonding affinity of HSA (C) during a c-ME experiment. (A) The surface concentration of immobilized HSA decreased only by about 1.1% per 10 h due to detachment from the Ge MIRE. The ability of cholate to act as detergent, and mechanical stress by c-ME might be the main reasons. (B) The maximum surface concentration of reversibly bonded cholate decreased by about 1.7% per 10 h. Detachment and denaturation of HSA might be the mean reasons for that. Surface concentrations were evaluated as described in the theoretical part. (C) Decrease of the bonding affinity of HSA due to the effects depicted by (A) and (B). Note that the large slope only results from expanded ordinate.

to get information of the HSA-cholate interaction only, cholate absorbance of the bulk has to be subtracted. Therefore, c-ME was also performed without HSA layer (Figure 5C). Figure 5D is the difference of the spectra shown in Figure 5B,C reflecting only the phase-resolved absorbance of cholate interacting with the HSA layer. The displacement of the bulk solution by the layer was taken into account according to Section 'Background compensation'.

Mean Spatial Orientation of Cholate Bonded to HSA. Figure 6 presents an expanded range of Figure 5D in the amide I/II and COO^- stretching region. The dichroic ratio of $\nu_s(COO^-)$ resulted in $R_{exp} = 1.78 \pm 0.13$. Under the same experimental conditions (Ge MIRE, $\theta = 45°$, $n_1 = 4.0$, $n_2 = 1.45$, $n_3 = 1.31$) a thin isotropic layer would result in $R_{iso,thin\ film} = 1.63 \pm 0.12$. Therefore, one may expect some spatial ordering of bonded cholate. According to Section 'Orientation measurements' the mean orientation of the transition moment of $\nu_s(COO^-)$, which has approximately the direction of the O−C−O bisector, forms an angle of $\Theta = (52.1 \pm 0.9)°$ with the normal to the MIRE (z-axis).

There is also a clear structural change of immobilized HSA induced by cholate bonding as visualized by the narrow band at 1656 cm^{-1}, which is generally assigned to α-helical structure. Since it appeared in-phase with the two carboxyl stretching vibrations $\nu_{as}(COO^-)$ at 1544 and $\nu_s(COO^-)$ at 1405 cm^{-1} of bonded cholate, an increase of α-helical structures evoked by cholate bonding to HSA is assumed. The dichroic ratio of this modulating component was $R_{exp}(\text{amide I},\alpha\text{-helix}_{mod}) = 1.87$. Compared to an isotropic distribution ($R_{iso,th} = 1.56$) this indicates an ordered adjustment of amide bondings involved in the bonding process of immobilized HSA and cholate. The total amount of amide groups showing this structural change can be estimated to 0.2% of all amide bondings of HSA by comparison of the total absorption of amide I of the HSA layer and the change of absorption due to cholate modulation. As the measured change of absorption is only due to a structural rearrangement and not by increase or decrease of HSA, the effect is mainly seen in the most structural sensitive amide I region and could not be detected in the amide II or amide III region. Amide II region is additionally overlapped by the strong modulated absorbance of $\nu_s(COO^-)$.

Stoichiometry of HSA/Cholate Interaction. Although quasi-stability of the protein layer was achieved by washing with PBS, as shown by Figure 3, the ability of cholate to act as detergent, caused still a very slow linear decrease of the surface concentration of HSA in the amount of 1.1% per 10 h. In order to evaluate the time course of the surface concentrations of HSA and cholate, pp and vp SBSR spectra were recorded after each vp−pp−vp modulation cycle. Data analysis was made according to sections "background compensation" and "determination of surface concentration". The time course of the surface concentrations of HSA and cholate bonded to adsorbed HSA are shown in Figure 7A,B, respectively. The stoichiometric ratio achieved at the beginning of c-ME was then evaluated by extrapolation of both curves to time zero by means of a linear regression. The resulting surface concentrations were found to be $\Gamma_{0,HSA} = (5.31 \pm 0.49) \times 10^{-12}$ mol cm^{-2}, and $\Gamma_{0,cholate} = (3.21 \pm 0.42) \times 10^{-11}$ mol cm^{-2}, leading to a ratio of 6.1 ± 1.0 cholate molecules per adsorbed HSA at a cholate bulk concentration of 5.0 mM. The resulting time course of stoichiometry is shown in Figure 7C. As a consequence, the bonding affinity of an immobilized HSA molecule was reduced from 6 to 5 cholate

molecules within 95 h, a fact that may be explained by denaturation of HSA due to aging or hydrodynamic stress by ME. It should be noted that $\Gamma_{0,HSA}$ differed in the limits of error from Γ_{HSA} as reported in section "characterization of the immobilized HSA layer", since $\Gamma_{0,HSA}$ was determined by linear regression and Γ_{HSA} by evaluation of single spectra measured with pp and vp incident light at the end of the procedure of HSA layer preparing.

Conclusions

In this work we had two goals: (i) demonstrating the capability of enhanced FTIR ATR spectroscopic techniques, such as concentration-modulated excitation (c-ME) and single-beam-sample-reference (SBSR) spectroscopy, to investigate specific interaction between a ligand and a receptor on a molecular level, and (ii) performing this analysis on a well investigated system of general interest like HSA, in order to show that additional information can be achieved by FTIR ATR spectroscopy (e.g., structural changes induced by the interaction of molecules).

ATR spectroscopy reaches optimum efficiency when applied to thin films and surfaces. Therefore, HSA was immobilized by adsorption to the germanium multiple internal reflection element (Ge-MIRE), being aware that this step is somewhat unnatural. Nevertheless, this system was very easy to handle, since HSA formed spontaneously a very stable monolayer at the Ge-MIRE surface. This is a prerequisite for c-ME, which is based on a periodic exchange of the bulk solution in contact with the HSA layer. Cholate at a concentration of 5 mM in PBS was used as specifically interacting ligand. Thus c-ME was performed by exposing the HSA layer repeatedly to 5 mM cholate in PBS during one-half-period of $T/2 = 4.9$ min, followed by a computer controlled exchange of the bulk by pure PBS in the second half-period.

It turned out that a stable baseline is of utmost importance, since measuring times in the range of 80−100 h were necessary to achieve sensitivities in the microabsorbance range. This high sensitivity is required for the study of structural changes in monolayers, which are induced by interaction with a ligand dissolved in the bulk environment. Measurements with parallel and perpendicular polarized light, as well as repeated checks of the stability of the whole system are included in the indicated measuring time. c-ME in combination with SBSR spectroscopy is significantly superior to conventional difference spectroscopy. ME techniques may relatively easily be adapted to any FTIR spectrometer. Possible applications are described in details in ref 9 and 13. Quantitative analysis of ME data is reported in ref 22.

As concluded from Figure 6, the peak-to-peak noise level of c-ME spectra is below 10 μAU. When working in such a sensitivity range, some effects which normally do not play a significant role have to be considered. Among them, one should note: (i) Displacement of bulk solution by the layer adsorbed to the MIRE. This point is of significant importance for the determination of the number of cholate bonding sites per HSA because c-ME spectra are dominated by absorbance bands resulting from periodic exchange of the bulk solution. Bonded cholate has to be evaluated by a scaled subtraction of the bulk. (ii) Instabilities in the progression of the experiment, such as detachment and denaturation of HSA. Procedures have been developed in order to correct the experimental data quantitatively for disturbances as just mentioned.

The second aim of this work, i.e., comparing our results with published data and getting insight into structural changes of HSA induced by cholate bonding, may be commented as follows: Stationary spectra of adsorbed HSA were recorded in the SBSR mode, which turned out to result improved compensation of buffer bands and laboratory atmosphere in the background. Quantification of the protein layer and comparison with a theoretical surface concentration, derived by geometrical considerations, gave strong evidence that the covering is close to a monolayer. During modulation measurements a loss of immobilized HSA was observed due to mechanical stress by c-ME, and due to the fact that cholate has qualities of a mild detergent.

Calculation of surface concentrations of HSA and cholate using corrected experimental data resulted in: $\Gamma_{0,HSA} = (5.31 \pm 0.49) \times 10^{-12}$ mol cm^{-2} and $\Gamma_{0,cholate} = (3.21 \pm 0.42) \times 10^{-11}$ mol cm^{-2}, respectively. Thus under equilibrium conditions between the HSA layer and a 5 mM cholate bulk solution the number of bonded cholate molecules per HSA molecule resulted in $\Gamma_{0,cholate}/\Gamma_{0,HSA} = 6.1 \pm 1.0$. The bonding capacity was reduced from 6 to 5 cholate per HSA within about 100 h, probably due to partial denaturation of HSA or due to a small amount of irreversible bonding of cholate to HSA. Published data obtained by equilibrium dialysis may be used for comparison.[7] Two bonding constants are reported, namely $K_1 = 3300$ with 2.8 sites, and $K_2 = 300$ with 12 sites. Moreover, 9.8 cholate per HSA were found at 5 mM cholate concentration in the bulk.

The molecular sites of HSA involved in the binding process to cholate are still not known. Nevertheless, there are two different types of bonding sites described, exhibiting dissimilar bonding constants.[7] Despite the negative net charge at pH 7.4, HSA exhibits an unequal distribution of charges on its surface with positively charged regions allowing negatively charged molecules to interact.[2] Moreover, cholate exhibits hydrophobic areas which could be able to interact with hydrophobic pockets in the HSA molecules, like it is known in case of fatty acids.[44] As a new finding, our c-ME experiments revealed a conformational change of HSA upon cholate bonding, i.e., an increase of α-helical content. This corresponds to published findings that cholate and deoxycholate may have a stabilizing effect on α-helical structures of synthetic peptides like poly-L-lysine.[45]

References and Notes

(1) Peters, T. *All about Albumin*: Academic Press: New York, 1995.
(2) Carter, D. C.; Ho, J. X. Structure of serum albumin. *Adv. Protein Chem.* **1994**, *45*, 153–203.
(3) Figge, J.; Rossing, T. H.; Fencl, V. The role of serum proteins in acid-base equilibria. *J. Lab. Clin. Med.* **1991**, *117*, 453–467.
(4) Shrake, A.; Finlayson, J. S.; Ross, P. D. Thermal stability of human albumin measured by differential scanning calorimetry. I. Effects of caprylate and N-acetyltryptophanate. *Vox Sang* **1984**, *47*, 7–18.
(5) Mura-Galelli, M. J.; Voegel, J. C.; Behr, S.; Bres, E. F.; Schaaf, P. Adsorption/desorption of human serum albumin on hydroxyapatite: A critical analysis of the Langmuir model. *Proc. Natl. Acad. Sci. U.S.A.* **1991**, *88*, 5557–5561.
(6) Jones, M. N.; Chapman, D. *Micelles, Monolayers, and Biomembranes*; Wiley-Liss: New York, 1995.
(7) Roda, A.; Cappelleri, G.; Aldini, R.; Roda, E.; Barbara, L. Quantitative aspects of the interaction of bile acids with human serum albumin. *J. Lipid Res.* **1982**, *23*, 490–495.
(8) Weber, C.; Strobl, W.; Krause, A.; Falkenhagen, D. Novel detoxification device to support patients with hepatic failure. *Int. J. Artif. Organs* **2002**, *25*, 687.
(9) Fringeli, U. P.; Günthard, H. H.; Baurecht, D. In *Infrared and Raman Spectroscopy of Biological Materials*; Gremlich, H. U., Yan, B., Eds.; Marcel Dekker: New York, 2000; pp 143−192.
(10) Kottke-Marchant, K.; Anderson, J. M.; Umemura, Y.; Marchant, R. E. Effect of albumin coating on the in vitro blood compatibility of Dacron arterial prostheses. *Biomaterials* **1989**, *10*, 147–155.
(11) SBSR ATR equipment was obtained from OPTISPEC, Rigistrasse 5, CH-8173 Neerach, Switzerland.
(12) Fringeli, U. P. In situ infrared attenuated total reflection membrane spectroscopy. In Mirabella, F. M., Ed.; *Internal Reflection Spectroscopy*; Marcel Dekker, New York, 1992; pp 255−324.

(13) Baurecht, D.; Reiter, G.; Hassler, N.; Schwarzott, M.; Fringeli, U. P. Application of Special FTIR ATR Techniques for Quantitative Structural Analysis of Thin Surface Layers. *Chimia* **2005**, *59*, 226–235.

(14) Mueller, M.; Kessler, B.; Lunkwitz, K. Induced Orientation of r-Helical Polypeptides in Polyelectrolyte Multilayers. *J. Phys. Chem. B* **2003**, *107*, 8189–8197.

(15) Mueller, M.; Rieser, T.; Lunkwitz, K.; Meier-Haack, J. Polyelectrolyte complex layers: a promising concept for antifouling coatings verified by in-situ ATR-FTIR spectroscopy. *Macromol. Rapid Commun.* **1999**, *20*, 607–611.

(16) Schneider, M. S. Grunwaldt Jan-Dierk; Baiker Alfons, Near-critical CO2 in mesoporous silica studied by in situ FTIR spectroscopy. *Langmuir* **2004**, *20* (7), 2890–9.

(17) Zimmermann, R.; Küttner, D.; Renner, L.; Kaufmann, M.; Zitzmann, J.; Müller, M.; Werner, C. Charging and structure of zwitterionic supported bilayer lipid membranes studied by streaming current measurements, fluorescence microscopy, and attenuated total reflection Fourier transform infrared spectroscopy. *Biointerphases* **2009**, *4*, 1.

(18) Popa, A. M.; Angeloni, S.; Bürgi, T.; Hubbell, J. A.; Heinzelmann, H.; Pugin, R. Dynamic perspective on the function of thermoresponsive nanopores from in situ AFM and ATR-IR investigations. *Langmuir* **2010**, *26* (19), 15356–65.

(19) Matijasevic, J.; Hassler, N.; Reiter, G.; Fringeli, U. P. In Situ ATR FTIR Monitoring of the Formation of Functionalized Mono- and Multilayers on Germanium Substrate: from 7-Octenyltrichlorosilane to 7-Carboxylsilane. *Langmuir* **2008**, *24*, 2588–2596.

(20) Urakawa, A.; Bürgi, T.; Baiker, A. Sensitivity enhancement and dynamic behavior analysis by modulation excitation spectroscopy: Principle and application in heterogeneous catalysis. *Chem. Eng. Sci.* **2008**, *63*, 4902–4909.

(21) Fringeli, U. P., Verfahren zur simultanen, digitalen phasenempfindlichen Detektion von zeitaufgelösten, quasi-gleichzeitig erfassten Datenarrays eines periodisch stimulierten Systems, Internationale Patent Publikation, PCT, WO 97/08598[1997].

(22) Baurecht, D.; Fringeli, U. P. Quantitative Modulated Excitation Fourier Transform Infrared (ME-FTIR) Spectroscopy. *Rev. Sci. Instrum.* **2001**, *72*, 3782–3792.

(23) Baurecht, D.; Porth, I.; Fringeli, U. P. A new method of phase sensitive detection in modulation spectroscopy applied to temperature induced folding and unfolding of RNase A. *Vib. Spectrosc.* **2002**, *30*, 85–92.

(24) Schwarzott, M.; Lasch, P.; Baurecht, D.; Naumann, D.; Fringeli, U. P. Electric Field-Induced Changes in Lipids Investigated by Modulated Excitation FTIR Spectroscopy. *Biophys. J.* **2004**, *86*, 285–295.

(25) Urakawa, A.; Wirz, R.; Bürgi, T.; Baiker, A. ATR-IR Flow-Through Cell for Concentration Modulation Excitation Spectroscopy: Diffusion Experiments and Simulations. *J. Phys. Chem. B* **2003**, *107*, 13061–13068.

(26) Wirz, R.; Bürgi, T.; Lindner, W.; Baiker, A. Absolute Configuration Modulation Attenuated Total Reflection IR Spectroscopy: An in Situ Method for Probing Chiral Recognition in Liquid Chromatography. *Anal. Chem.* **2004**, *76*, 5319–5330.

(27) Harrick, N. J. *Internal Reflection Spectroscopy*; Harrick Sci. Corp.: Ossining, NY, 1979.

(28) Fringeli, U. P.; Baurecht, D.; Bürgi, T.; Siam, M.; Reiter, G.; Schwarzott, M.; Brüesch, P., ATR spectroscopy of thin films. In *Handbook of Thin Film Materials*; Nalwa, H. S., Ed.; Academic Press: New York, 2002; Vol. 2, Chapter 4, pp191−229.

(29) Schwarzott, M.; Engelhardt, H.; Klühspies, T.; Baurecht, D.; Naumann, D.; Fringeli, U. P. In Situ FTIR ATR Spectroscopy of the Preparation of an Oriented Monomolecular Film of Porin Omp32 on an Internal Reflecting Element by Dialysis. *Langmuir* **2003**, *19*, 7451–7459.

(30) Claesson, P. M.; Blomber, E.; Fröberg, J. C.; Nylander, T.; Arnebrant, T. Protein interactions at solid surfaces. *Adv. Colloid Interface Sci.* **1995**, *57*, 161–227.

(31) Zoungrana, T.; Findenegg, G. H.; Norde, W. Structure, Stability, and Activity of Adsorbed Enzymes. *J. Colloid Interface Sci.* **1997**, *190*, 437–448.

(32) Malmsten, M.; Muller, D.; Lassen, B. Sequential adsorption of human serum albumin (HSA), immunoglobulin G (IgG) and fibrinogen (Fgn) at HMDSO Plasma Polymer Surfaces. *J. Colloid Interface Sci.* **1997**, *193*, 88–95.

(33) Garrett, Q.; Milthorpe, B. K. Human serum albumin adsorption on hydrogel contact lenses in vitro. *Invest. Ophthalmol. Vis. Sci.* **1996**, *37*, 2594–2602.

(34) Buijs, J.; Norde, W. Lichtenbelt, J.W.Th. Changes in the secondary structure of adsorbed IgG and F(ab′)2 studied by FTIR spectroscopy. *Langmuir* **1996**, *12*, 1605–1613.

(35) Hlady, V.; Buijs, J. Protein adsorption on solid surfaces. *Curr. Opinion Biotechnol.* **1996**, *7*, 72–77.

(36) Sukhishvili, S. A.; Granick, S. Adsorption of human serum albumin: Dependence on molecular architecture of the oppositely charged surface. *J. Chem. Phys.* **1999**, *110*, 10153–10161.

(37) Malmsten, M. Protein adsorption at phospholipid surfaces. *J. Colloid Interface Sci.* **1995**, *172*, 106–115.

(38) Ball, V.; Huetz, P.; Elaissari, A.; Cazenave, J.-P.; Voegel, J.-C.; Schaaf, P. Kinetics of exchange processes in the adsorption of proteins on solid surfaces. *Proc. Natl. Acad. Sci. U.S.A.* **1994**, *91*, 7330–7334.

(39) Haynes, C. A.; Norde, W. Globular proteins at solid/liquid interfaces. *Colloids Surf. B: Biointerfaces* **1994**, *2*, 517–566.

(40) Kurrat, R.; Prenosil, J. E.; Ramsden, J. J. Kinetics of human and bovine serum albumin adsorption at silica-titania surfaces. *J. Colloid Interface Sci.* **1997**, *185*, 1–8.

(41) Chirgadze, Yu. N.; Brazhnikov, E. V. Intensities and other spectral parameters of infrared amide bands of polypeptides in the a-helical form. *Biopolymers* **1974**, *13*, 1701–1712.

(42) Ramsden, J. J. Concentration scaling of protein deposition kinetics. *Phys. Rev. Lett.* **1993**, *71*, 295–298.

(43) Roda, A.; Hofmann, A. F.; Mysels, K. J. The Influence of Bile Salt Structure on Self-association in Aqueous Solutions. *J. Biol. Chem.* **1983**, *258*, 6362–6370.

(44) Curry, S.; Mandelkow, H.; Brick, P.; Franks, N. Crystal structure of human serum albumin complexed with fatty acid reveals an asymmetric distribution of binding sites. *Nat. Struct. Biol.* **1998**, *5*, 827–835.

(45) D'Alagni, M.; D'Archivio, A. A.; Giglio, E. On the Interaction of Polypeptides with Bile Salts or Bilirubin-IXa. *Biopolymers* **1993**, *33*, 1553–1565.

(46) Fringeli, U. P.; Apell, H.-J.; Fringeli, M.; Läuger, P. Polarized infrared absorption of Na^+/K^+-ATPase studied by attenuated total reflection spectroscopy. *Biochim. Biophys. Acta* **1989**, *984*, 301–312.

JP105870Z